Nanomechanical properties of silicon surfaces nanostructured by excimer laser

2010 Sci. Technol. Adv. Mater. 11 025003

(http://iopscience.iop.org/1468-6996/11/2/025003)

IOP Publishing Science and Technology of Advanced Materials
Sci. Technol. Adv. Mater. **11** (2010) 025003 (8pp) doi:10.1088/1468-6996/11/2/025003

Nanomechanical properties of silicon surfaces nanostructured by excimer laser

Prashant Kumar[1] **and M S R N Kiran**[2]

[1] Chemistry and Physics of Materials Unit (CPMU), Jawaharlal Nehru Centre for Advanced Scientific Research (JNCASR), Jakkur P O, Bangalore 560064, India
[2] Department of Materials Engineering, Indian Institute of Science (IISc), Bangalore 560012, India

E-mail: prashantkumar@jncasr.ac.in

Received 18 December 2009
Accepted for publication 17 March 2010
Published 13 May 2010
Online at stacks.iop.org/STAM/11/025003

Abstract
Excimer laser irradiation at ambient temperature has been employed to produce nanostructured silicon surfaces. Nanoindentation was used to investigate the nanomechanical properties of the deformed surfaces as a function of laser parameters, such as the angle of incidence and number of laser pulses at a fixed laser fluence of 5 J cm^{-2}. A single-crystal silicon [311] surface was severely damaged by laser irradiation and became nanocrystalline with an enhanced porosity. The resulting laser-treated surface consisted of nanometer-sized particles. The pore size was controlled by adjusting the angle of incidence and the number of laser pulses, and varied from nanometers to microns. The extent of nanocrystallinity was large for the surfaces irradiated at a small angle of incidence and by a high number of pulses, as confirmed by x-ray diffraction and Raman spectroscopy. The angle of incidence had a stronger effect on the structure and nanomechanical properties than the number of laser pulses.

Keywords: excimer laser, nanostructuring, nanocrystallinity, nanoindentation

1. Introduction

The surface modification of semiconductors, e.g. silicon, has great fundamental and technological importance. It is achieved by various methods, such as chemical etching and different types of high-energy beam irradiation employing high-power laser beams. Silicon is a versatile material, which is being used very extensively in the electronic industry for most of the semiconducting applications. It exhibits a range of attractive properties, such as high melting/boiling point, thermodynamic and chemical stability, and semiconducting properties [1]. Laser beam interaction with silicon has been a major focus of interest of the research community because modified silicon surfaces exhibit novel functional properties [2–15]. The Nd:YAG [16–18], excimer [19, 20] and CO_2 lasers are typically used for these purposes. Semiconducting materials with a low thermal conductivity and a high mechanical stability are required for microelectromechanical systems (MEMS) [21, 22]. One of the most important advantages of nanocrystalline silicon is that it has an increased stability over amorphous silicon (a-Si)—a candidate MEMS material—for one of the reasons being its lower hydrogen concentration. Producing silicon surfaces with desired physical properties (such as optical, electrical and thermal behaviors) without sacrificing their mechanical strength is a current technological challenge. Excimer-laser-induced nanostructuring and surface modification still attract attention owing to their potential for material modification and good process control [23].

Studies on the effects of laser processing parameters on mechanical properties of silicon are very rare in the literature. To date, only porous silicon as-prepared by a chemical route has been characterized in terms of its mechanical properties [24]. An extensive research on the excimer-laser-induced nanostructuring of surfaces has been carried out by Kumar *et al.* [25, 26]. Such laser-nanostructured silicon surfaces exhibited strong light absorption and photoluminescence due to their porous structure produced through catastrophic damage [27]. It is imperative to perform a systematic study of nanomechanical properties of excimer-laser-fabricated nanostructured silicon, as reported in this article.

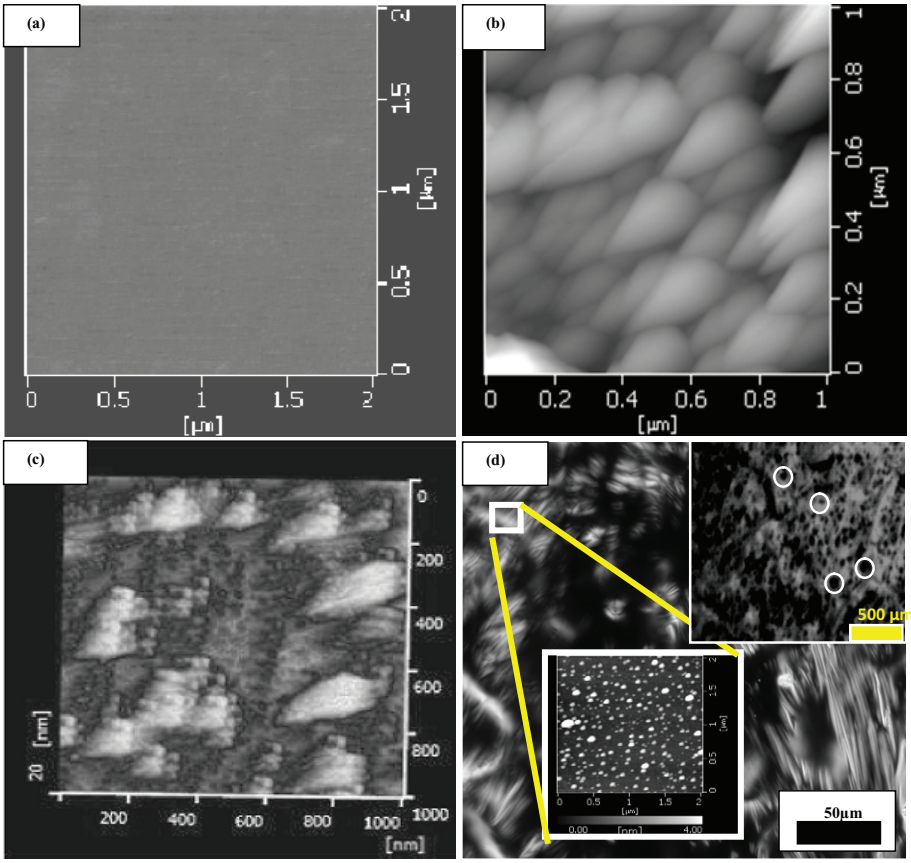

Figure 1. AFM images in DFM mode for (a) untreated silicon and for silicon laser irradiated at a fluence of 5 J cm^{-2} and incident angle of 90° by (b) 1 pulse and (c) 8 pulses; (d) shows optical micrograph obtained after application of 100 pulses. The top-right inset shows a large-area optical image revealing a significant porosity in laser-treated surfaces, and the bottom inset shows an AFM image showing nanoparticle formation.

2. Experimental details

The surfaces of [311]-oriented silicon wafers were irradiated by a KrF excimer laser (Compex Pro 201F, Lambda Physik, Germany) with a wavelength of 248 nm and a peak energy of 700 mJ in a 30 ns pulse. The surfaces were cleaned ultrasonically in acetone, isopropyl alcohol and distilled water each for 15 min and dried in an oven at 80 °C for 20 min. The laser repetition rate was maintained at 1 Hz for all experiments. The incident laser fluence was kept constant at 5 J cm^{-2} and the surfaces were irradiated by 1 to 100 pulses. The angle of incidence of a laser beam on a silicon surface was fixed at 20, 30, 45 or 90°.

The catastrophic damage after irradiation was monitored using an optical microscope (Olympus Model MX51). Microstructural changes were observed with an atomic force microscope (AFM, SPA 400 of SII Inc, Japan), operating in the intermittent contact dynamic force microscope (DFM) mode. The extent of crystallinity was determined by Raman spectroscopy (He–Ne laser excitation) and x-ray diffraction (XRD, Co-K_α radiation, $\lambda = 1.7902$ Å) measurements carried out at room temperature.

Mechanical properties of virgin silicon and laser-treated silicon surfaces, after various numbers of shots at various incident angles, have been investigated using a Hysitron Triboscope indentation system (Minneapolis, MN, USA). A three-sided pyramidal Berkovich tip of 100 nm diameter was used in this study. A maximum load (P_{max}) of up to 8 mN was used. In all cases, the rates of loading and unloading were set such that the loading and unloading times were both 10 s with a pause of 10 s at P_{max}. Load (P) versus depth of penetration (h) was recorded and analyzed to extract Young's modulus (E) and hardness (H) using the Oliver and Pharr method [28, 29]. Images of the indents were captured using the same indenter in the scanning probe microscopy (SPM) mode. The SPM imaging of the surfaces was conducted before and after each indent to perform indentations in relatively smooth, defect-free regions.

3. Results and discussion

The excimer laser irradiation of single-crystal silicon surfaces with a laser fluence of 5 J cm^{-2} was an extreme condition that caused severe damage to the surface. When silicon interacted with a laser, it underwent nonequilibrium changes resulting in catastrophic damage. As is evident from the optical images, the untreated silicon surface (figure 1(a)) was significantly roughened and bundled fiber-like microstructures were formed (figure 1(d)). At the incident angle of 90°, and for 1 shot, the size of nanoparticles on the surface was

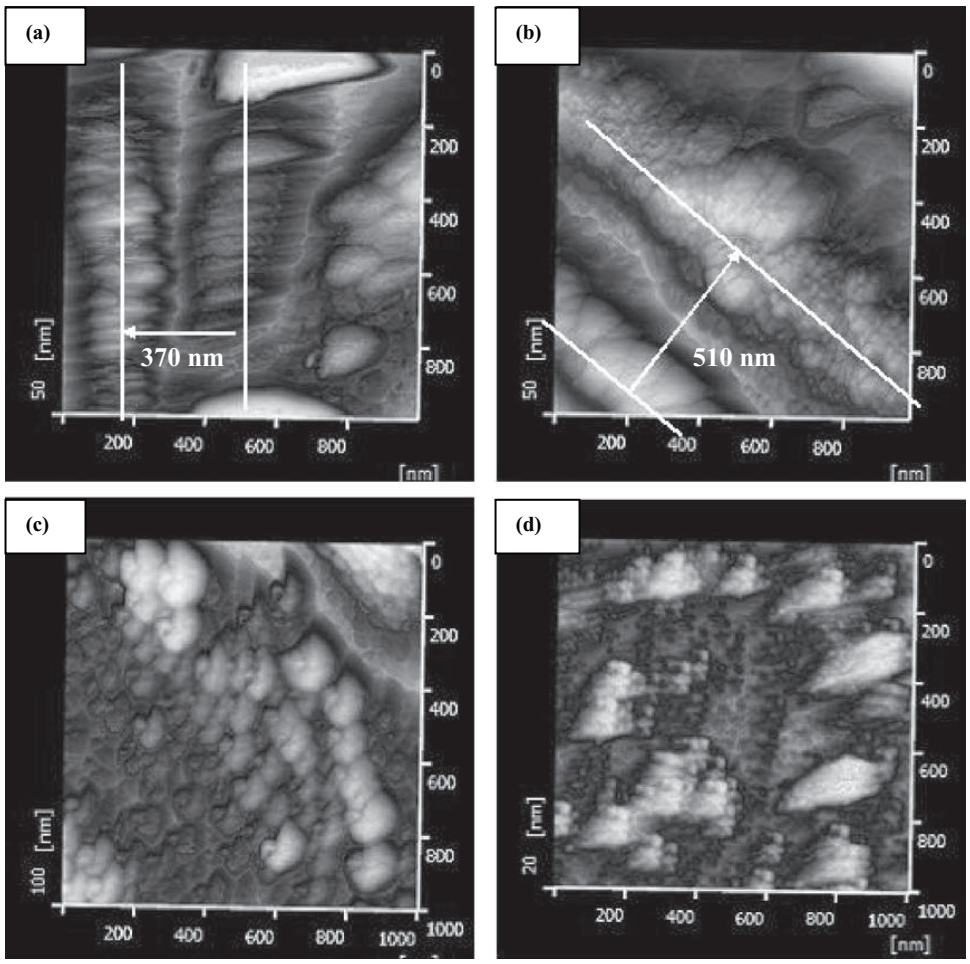

Figure 2. AFM images in DFM mode of the silicon surface nanostructured by 8 laser pulses at fluence of 5 J cm^{-2} and incident angles of (a) 20°, (b) 30°, (c) 45° and (d) 90°.

approximately 300 nm (figure 1(b)), which reduced to 40–60 nm after 100 shots (figure 1(d)). At 8 shots, silicon condensed into clusters, as shown in figure 1(c). A larger number of laser pulses resulted in a higher extent of nanostructuring and hence a smaller nanoparticle size. The presence of pores in the modified silicon surfaces irradiated by 8 pulses at the 90° angle of incidence is shown in the upper right inset of figure 1(d). Few pores are indicated by circles for better identification, and the pore size varies from 10 nm to 300 μm. An almost 50–90% porosity was achieved by varying the incident angle of laser beam. Various types of pores, i.e., micropores, mesopores and macropores, were observed in our experiments.

To investigate the effect of incident angle on surface nanostructuring, the angle was varied from 20 to 90°. At an incident angle of 20°, it is clear from figure 2(a) that an anisotropic growth feature is present with nanostripes aligned in the direction of the laser beam. At 30°, however, more interesting growth features were observed in the form of nanowires oriented in the direction of the laser beam and consisted of minute nanoparticles, as shown in figure 2(b). At 45°, the anisotropy in the growth features was reduced (figure 2(c)), and at 90°, the growth was almost isotropic (figure 2(d)). At 20 and 30°, the separations between two self-organized linear features were 370 and 510 nm, respectively. The formation of such self-organized nanostructures is part of an independent on-going research.

The effect of laser irradiation on the evolution of microstructures on single-crystal silicon surfaces is depicted in figure 3. Figure 3(a) shows the variation in grain size distribution with the number of laser shots; 250–300 grains were used to evaluate the grain size distribution of the modified surfaces in a $10 \times 10\ \mu$m^2 area. The average grain size was about 180 nm for 1 shot and its distribution was monomodal. For 8 shots, however, the average grain size reduced to 110 nm and the distribution became bimodal. For 100 shots, the grain size further reduced to 80 nm, retaining the bimodal distribution. Such a bimodal distribution might be due to further fragmentation of formed minute grains by successive laser bombardment. The effect of the incident angle of the laser beam on the grain size distribution of silicon surfaces is shown in figure 3(b). Laser irradiations at 90 and 45° resulted in a coarse grain microstructure with a size distribution wider than those for 30 and 20°.

XRD patterns of the laser-irradiated surfaces are shown in figure 4. Single-crystal silicon exhibited a very sharp peak at $2\theta = 66.4°$. Laser-irradiated surfaces showed a peak at the

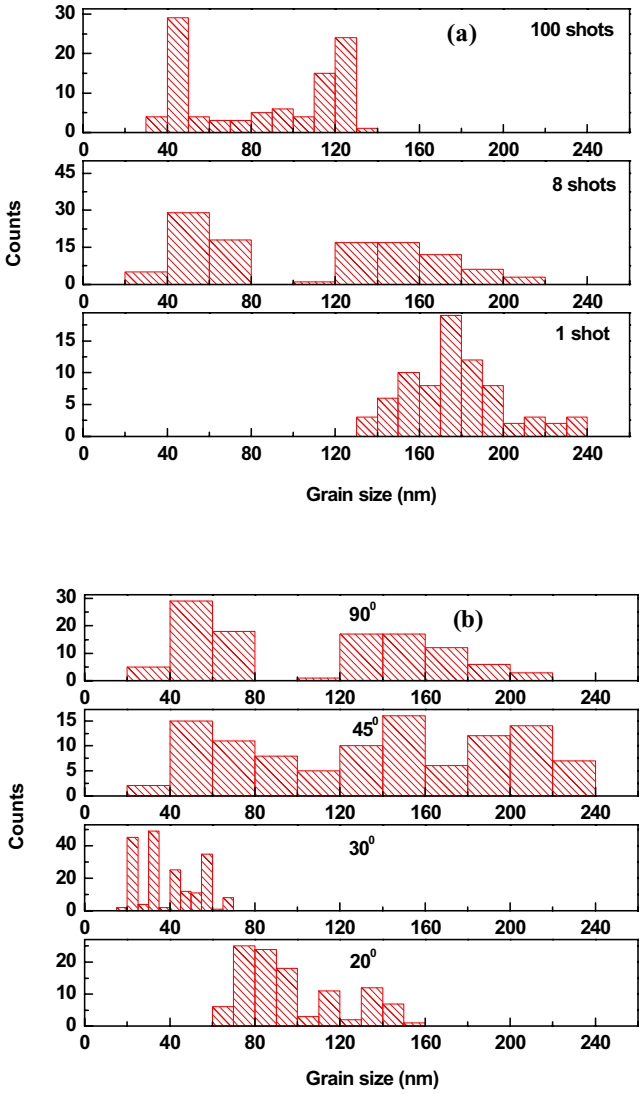

Figure 3. Variation in grain size of laser-treated surfaces with (a) number of shots and (b) angle of incidence.

same position but with a higher full width at half maximum (FWHM), indicating that the surfaces lost their long-range crystalline order and became nanocrystalline or amorphous; the FWHM increased with the number of laser pulses. No peaks from silicon oxide were observed in the XRD patterns, indicating the lack of oxidation of the modified surfaces. The crystallite size was reduced from 30 to 10 nm with increasing number of pulses from 1 to 100, as estimated with Scherer's equation. In laser–material interaction, the surface locally heats up to $\sim 3\,000\,^{\circ}\mathrm{C}$ and then cools down to room temperature within microseconds after laser pulse application. Thus, the surface experiences ultrafast cooling that could be responsible for the observed amorphization. We would also note that when significant damage occurs, microsized and nanosized features are formed on the surface. Each microstrand in a bundled fiber-like structure, for example, consists of many nanograins, as demonstrated in figure 1(d). An example of this surface feature is also shown in figure 2(b), where each nanowire consists of grains that are much smaller than the wire diameter.

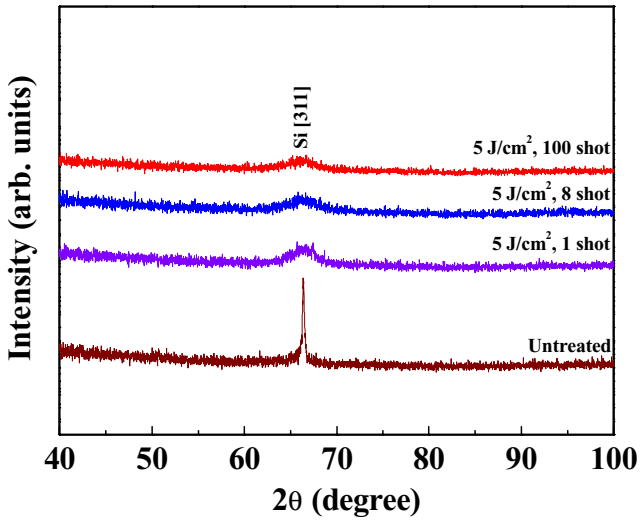

Figure 4. XRD patterns for (a) untreated silicon and silicon irradiated at 90° by (b) 1 pulse, (c) 8 pulses and (d) 100 pulses.

Raman spectra of excimer-laser-nanostructured silicon surfaces showed that crystallite size is smaller at a relatively low incident angle than at a higher incident angle, as shown in figure 5. This size change was revealed in the AFM images shown in figure 2, and it resulted in the broadening of the characteristic silicon Raman peak at $518\,\mathrm{cm}^{-1}$. The extent of surface nanocrystallization increased with the number of laser pulses as confirmed by the broadening of the Raman peak. There was no broadening for the Raman peak centered at $300\,\mathrm{cm}^{-1}$. This peak is 20 times weaker than the $518\,\mathrm{cm}^{-1}$ line. Both peaks are due to the phonon modes of the Si substrate. Preliminary results suggest the following two main contributions to these Raman peaks: transverse optical phonon (TO) and grain boundary defects, such as stacking faults. These two contributions result in the broadening of the $518\,\mathrm{cm}^{-1}$ line toward the low-energy side and thus an asymmetrical peak shape. This asymmetry is associated with a grain size distribution that can generate tensile strain on the surface [30].

To perform a meaningful nanoindentation of a modified, nanostructured silicon surface, it is essential to locate the damaged region. This was accomplished by using the *in situ* SPM imaging capability of the Triboindenter. An area of $100\,\mu\mathrm{m}^2$ was scanned by SPM, and the region with a minimum surface roughness was selected for indentation. Figure 6(a) shows the load-displacement curves for the untreated and laser-irradiated silicon surfaces at different numbers of pulses. A pop-out (sudden material expansion) occurred in the unloading curve for the untreated silicon surface at $1760\,\mu\mathrm{N}$ load and at 104 nm depth. This type of behavior was not observed for any of the laser-treated silicon surfaces. From figure 6(a), it is clear that the initial part of unloading is purely elastic, because it follows the power law relation (equation (2)). The loading curve can be fitted with the power law relation,

$$P = \alpha h^m \tag{1}$$

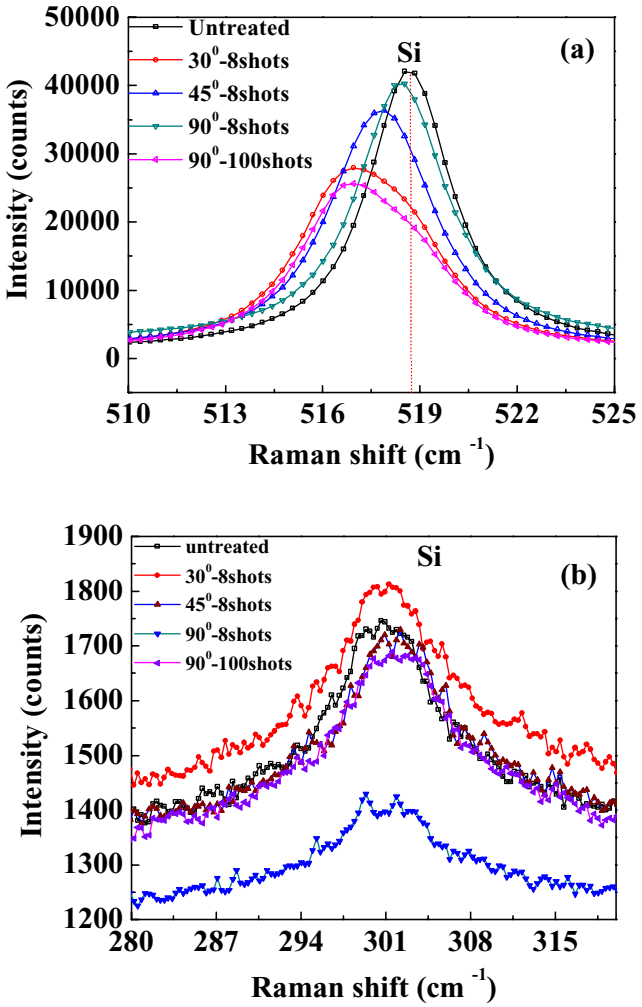

Figure 5. Raman spectra for silicon surfaces irradiated at various angles of incidence and numbers of laser pulses.

and the unloading curve can be expressed as

$$P = \alpha\,(h - h_{\mathrm{f}})^{m}. \tag{2}$$

Here, P is the indenter load, h is the elastic displacement of the indenter, h_{f} is the final depth, and α and m are fitting constants. The value of m for the Berkovich tip is typically 1.5.

It has already been well established that the inelastic deformation in silicon under nanoindentation is mainly caused by phase transformations and the contributions from other deformation mechanisms. Thus, the bifurcation from the elastic curve shown in figure 6(a) indicates that a phase transformation has occurred. A pop-out can occur after the bifurcation. Chang and Zhang [31] indicated that the onset of phase transformation during unloading occurs once the contact pressure reaches the critical value (for the phase transition from Si-II to Si-III/Si-XII and/or to amorphous phases) and is independent of peak indentation load or of loading/unloading rate. The pop-out effect is a consequence of a phase transformation from metallic Si–II to either Si–III or Si–XII, accompanied by a sudden volume increase and hence the uplift of the material surrounding an indenter. Interestingly, the unloading part after the pop-out can also

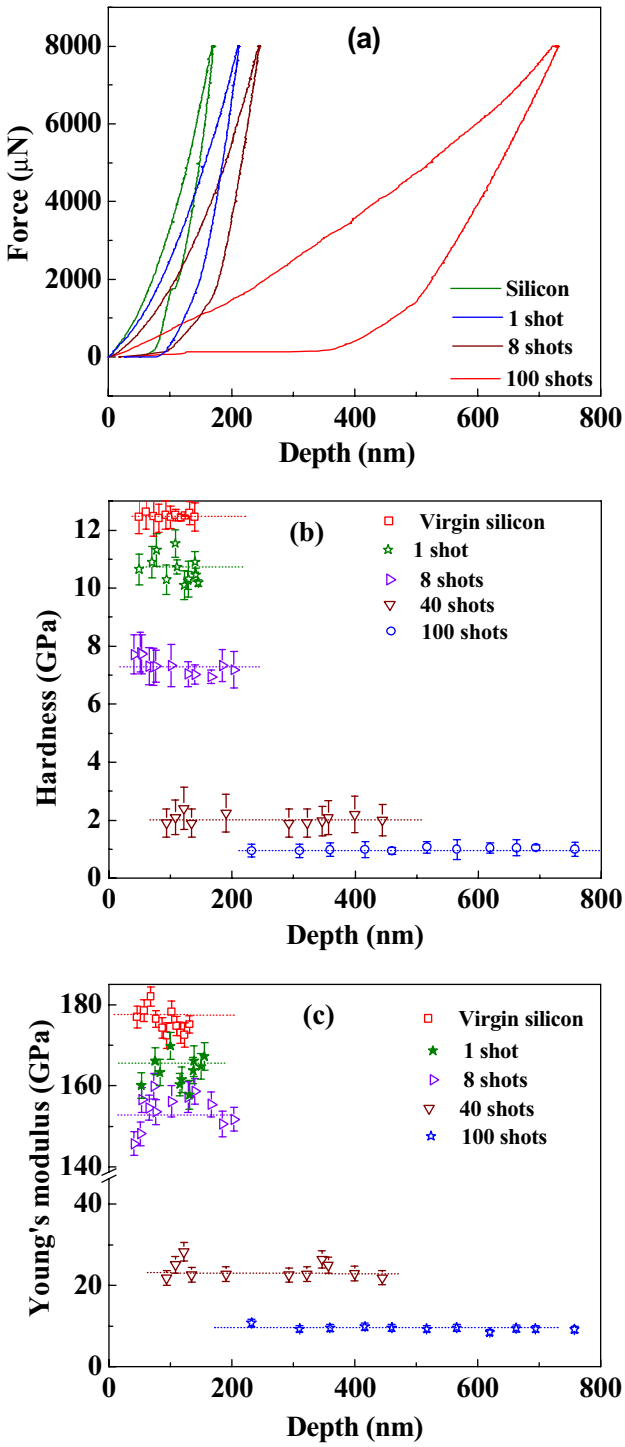

Figure 6. Nanoindentation data for 90° incident angle and various numbers of pulses: (a) force versus depth, (b) hardness versus depth and (c) Young's modulus versus depth.

be fitted with the power law relation, indicating that the unloading process after a pop-out is purely elastic. The absence of pop-out in the unloading part for the laser-treated silicon surfaces is interesting. It could be attributed to the phase transformation of silicon from a single crystal to an amorphous/nanocrystalline phase as a result of laser irradiation.

Figure 6(a) reveals a systematic load-displacement (L-D) curves variation with varying number of pulses. After 1 pulse,

a negligible load-displacement curve difference was seen as compared with virgin silicon, whereas a significant difference in load-displacement curve was observed for 100 pulses. Although the loading and unloading rates were the same ($\sim$800 μN s^{-1}) in all experiments, the slope of the loading curve varied significantly after different numbers of pulses. The indenter penetrated into the material without any resistance after irradiation, indicating that the material became very soft because of rapid-cooling-induced surface porosity.

Figure 6(b) presents a typical plot of hardness and Young's moduli of laser-treated surfaces (laser fluence of 5 J cm^{-2} and incident angle of 90°) versus indentation depth at various numbers of pulses. The hardness of untreated silicon was $\sim$ 12.8 GPa and decreased to 10.5, 7, 2 and less than 1 GPa after laser irradiations at 1, 8, 40 and 100 shots, respectively. Clearly, the extent of surface damage increased with the number of pulses, and a catastrophic surface damage was observed after 100 shots. The variation in the Young's modulus of the damaged surface with the number of pulses is shown in figure 6(c). The modulus of untreated silicon was $\sim$ 180 GPa and decreased to 165, 150, 22 and 10 GPa for 1, 8, 40 and 100 shots, respectively. Modulus is a measure of stiffness—the higher the modulus, the stiffer the material. This does not, however, guarantee good deformability or energy absorption before fracture. We observed that more laser pulses induced heavier damage, larger porosity and smaller grain sizes. This type of nanostructuring gradually softens the surface.

Figure 7(a) shows the load-displacement curves for various angles of incidence and 8 laser pulses. The observed behavior is different from the power law relation for surfaces irradiated at smaller angles of incidence, namely, 20, 30 and 45°. At 20°, the unloading part of the load-displacement curve shows a sudden increase in the elastic recovery rate of the indented material. This recovery rate was lower for surfaces irradiated at 30 and 45° than for the surface irradiated at 20°. This type of unloading behavior was not observed for the surfaces irradiated by different numbers of pulses. Figures 6(a) and 7(a) suggest that the angle of incidence has a more profound effect on the surface modification than the number of pulses, that is, 100 shots at 90° and 8 shots at 20° resulted in similar hardnesses and moduli. This could be due to the fact that laser energy is more localized at 90°, which resulted in the molten the material and an immediate solidification. However, at lower angles of incidence, the damage area was a significantly elongated ellipse. The energy delivered to the material was invested in material movement along the laser beam. This was corroborated by the optical micrographs. A large and deep eroded trench was observed at lower angles of incidence, but shallow ripples occurred after 90° irradiation. Smaller angles of incidence resulted in an improved porosity. Therefore, instead of increasing the number of laser pulses, one could reduce the incident angle to achieve improved material properties (compactness).

Figure 7(b) presents a typical plot of hardness and Young's modulus of laser-treated surfaces (laser fluence of 5 J cm^{-2} and 8 pulses) with indentation depth for various angles of incidence. The hardness of untreated silicon was

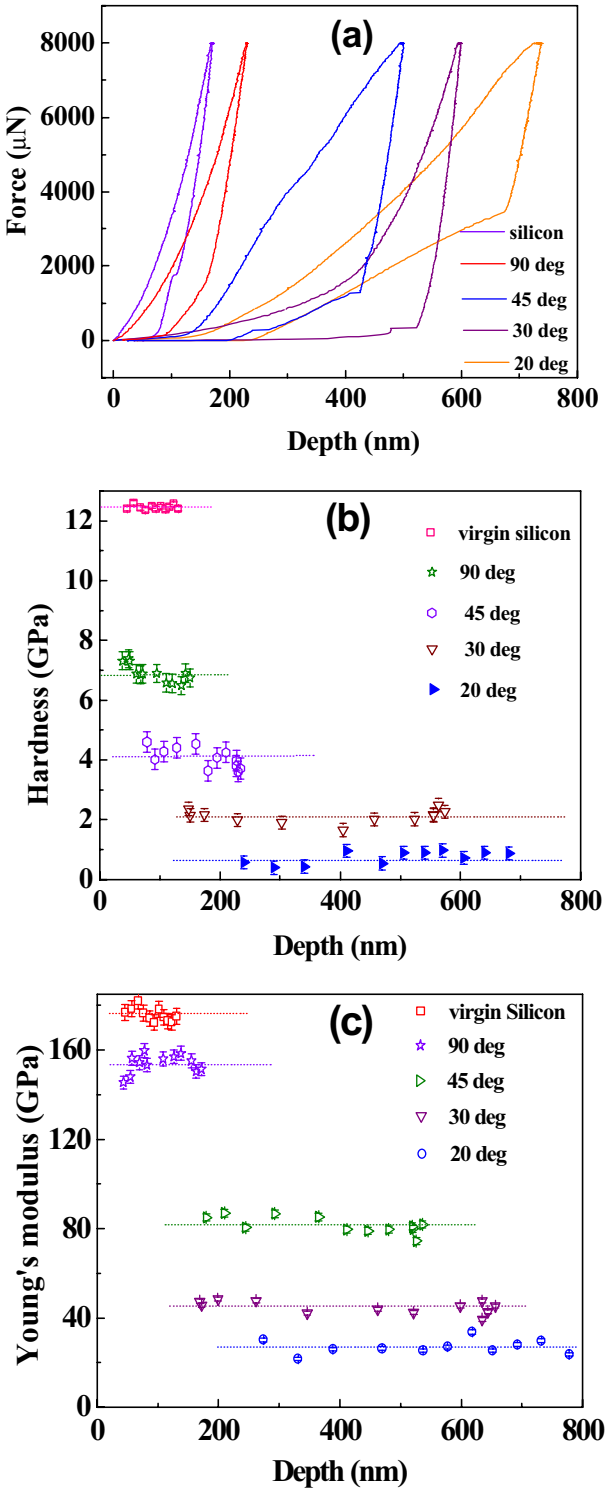

Figure 7. Nanoindentation data for silicon irradiated by 8 pulses at various angles: (a) force versus depth, (b) hardness versus depth and (c) Young's modulus versus depth.

$\sim$ 12.8 GPa and decreased to 7, 4, 2 and less than 1 GPa after laser irradiations at 90, 45, 30 and 20°, respectively. It was clearly observed that the surface damage increased with decreasing angle of incidence. The variation in the Young's modulus of the damaged surfaces with the angle of incidence is shown in figure 7(c). The modulus of untreated silicon

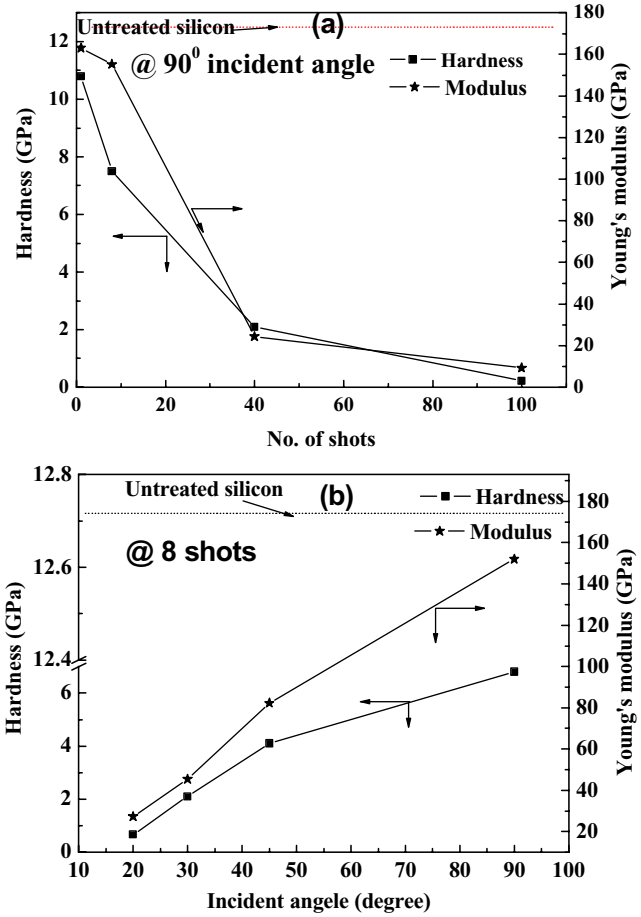

Figure 8. Variations of hardness and Young's modulus with (a) number of pulses and (b) angle of incidence.

was ∼ 180 GPa and decreased to 150, 80, 42 and 22 GPa for 90, 45, 30 and 20° incident angles, respectively. Linear profiles (ripples) were observed in the direction of the laser beam at small irradiation angles. Each ripple consists of minute nanoparticles, and its growth is highly anisotropic at small angles of incidence. As the incident angle gradually increased to 45°, the anisotropy decreased and vanished at 90°. Moreover, the surface layers were removed (ablated) at 90° but not at angles smaller than 90°, at which material was instead redistributed on the surface. Very few remaining nanoparticles can be seen on the silicon surface for the 90° incident angle. Figure 8 shows the hardnesses and moduli of laser-irradiated silicon surfaces as a function of the laser parameters.

In general, hardness should be large for reduced grain sizes up to a certain limit (∼ 10 nm, Hall-Petch effect). However, a small hardness was observed for small grains in this study. Such an inverse Hall-Petch behavior was typically seen for grains smaller than 10 nm, which is not the case here. Such an anomaly can be attributed to the high porosity of the excimer-laser-damaged silicon surfaces.

4. Conclusion

Single-crystal silicon surfaces have been modified using a KrF excimer laser at a laser fluence of 5 J cm^{-2}. A systematic investigation was carried out to explore the effects of the number of laser pulses and incident angle on the nanomechanical properties of the modified silicon surfaces. The porosity and grain size of the modified silicon surfaces were controlled by varying the laser parameters. We found that the incident angle of laser irradiation has a more profound effect on the modification of silicon surfaces than the number of laser pulses as far as nanomechanical properties are concerned.

Acknowledgments

The authors acknowledge the support and encouragement from Dr M Ghanashyam Krishna from School of Physics, University of Hyderabad. The excimer laser facilities of School of Physics, UOH were used for the present experiments. We are also grateful to Professor U Ramamurty, Department of Materials Engineering, Indian Institute of Science, for allowing us to use the nanoindentation system. MSRNK acknowledges the Dr D S Kothari fellowship of the University Grants Commission, Government of India. The authors also acknowledge financial support from Department of Science and Technology (DST).

References

[1] Trtica M S and Gakovic B M 2003 *Appl. Surf. Sci.* **205** 336
[2] Koshida N (ed) 2009 *Device Applications of Silicon Nanocrystals and Nanostructures* (NY: Springer Science and Business Media)
[3] Gaburro Z, Bettotti P, Daldosso N, Ghulinyan M, Navarro-Urrios D, Melchiorri M, Riboli F, Saiani M, Sbrana F and Pavesi L 2006 *Nanostructured Silicon for Photonics* Materials Science Foundation (*Monograph Series*) Vol 27–28 (Switzerland: Trans. Tech Publication Inc.)
[4] Diener J, Künzner N, Gross E, Kovalev D and Fujii M 2005 *Phys. Status Solidi* a **202** 1432
[5] Bettotti P, Cazzanelli M, Dal Negro L, Danese B, Gaburro Z, Oton C, Vijaya Prakash G and Pavesi L 2002 *J. Phys.: Condens. Matter* **14** 8253
[6] Fauchet P M, Tsybeskov L, Duttagupta S P and Hirschman K 1997 *Thin Solid Films* **297** 254
[7] Stefano L D, Moretti L, Rendina I, Rossi A M and Tundo S 2004 *Appl. Opt.* **43** 167
[8] Grigoras K, Krotkus A, Pacebutas V and Simkiene I 1998 *Proc. SPIE* **3580** 158
[9] Canham L T, Cox T I, Loni A, Simons A J and Blacker R S 2002 *US Patent* 6380550
[10] Dimova-Malinovska D 2006 *Application of Stain Etched Porous Silicon in Solar Cells and Light Emitting Diodes* (Netherlands: Springer)
[11] Rossi A M, Borini S, Boarino L and Amato G 2003 *Phys. Status Solidi* a **197** 284
[12] Lang W, Steiner P and Sandmaier H 1995 *J. Micromech. Microeng.* **5** 175
[13] Salonen J, Kaukonen A M, Hirvonen J and Lehto V-P 2008 *J. Pharm. Sci.* **97** 632
[14] Jaguiro P, Katsuba P, Lazarouk S and Smirnov A 2007 *Acta Phys. Pol.* A **12** 1031
[15] Pavesi L and Guardini R 1996 *Braz. J. Phys.* **26** 151
[16] Fang Z, Hu M, Zhang W, Zhang X and Yang H 2008 *J. Mater. Sci.: Mater. Electron.* **19** 1128
[17] Wolf A and Brendel R 2006 *Thin Solid Films* **513** 385

[18] Lee C, Kim D-Y, Kim J-H, Lee K-C and Hui C-S 2005 *J. Electron. Mater.* **34** 132
[19] Duttagupta S P and Fauchet P M 1997 *Properties of Porous Silicon* ed L T Canham (London: INSPEC) p 132
[20] Harzic R L, Schuck H, Sauer D, Anhut T, Riemann I and König K 2005 *Opt. Express* **13** 6651
[21] Weingartner M, Elschner R and Bostonjoglo O 1999 *Appl. Surf. Sci.* **138–139** 499
[22] Yoo J H, Jeong S H, Mao X L, Greif R and Russo R E 2000 *Appl. Phys. Lett.* **76** 783
[23] Mariucci L, Pecora A, Carluccio R and Fortunato G 2001 *Thin Solid Films* **383** 39
[24] Pedraza A J, Fowlkes J D, Jesse S, Mao C and Lowndes D H 2000 *Appl. Surf. Sci.* **168** 251
[25] Krishna M G and Kumar P 2009 *Emerging Nanotechnology for Manufacturing* ed W Ahmed and M J Jackson (Oxford: Elsevier Sciences)
[26] Kumar P, Krishna M G and Bhattacharya A 2009 *J. Nanosci. Nanotechnol.* **9** 3224
[27] Kumar P, Krishna M G and Bhattacharya A K 2009 *AIP Conf. Proc.* **1147** 244
[28] Oliver W C and Pharr G M 1992 *J. Mater. Res.* **7** 1564
[29] Oliver W C and Pharr G M 2004 *J. Mat. Res.* **19** 3
[30] Kanzaway Y, Hayashiz S and Yamamoto K 1996 *J. Phys.: Condens. Matter* **8** 4823
[31] Chang L and Zhang L C 2009 *Acta Mater.* **57** 2148